OPTICAL CONTINUUM AND EMISSION-LINE VARIABILITY OF SEYFERT 1 GALAXIES

BRADLEY M. PETERSON, IGNAZ WANDERS,[1] RAY BERTRAM,[2] JAMES F. HUNLEY,
RICHARD W. POGGE, AND R. MARK WAGNER[2]

Department of Astronomy, The Ohio State University, 174 West 18th Avenue, Columbus, OH 43210-1106; peterson@astronomy.ohio-state.edu,
jhunley@astronomy.ohio-state.edu, pogge@astronomy.ohio-state.edu

ABSTRACT

We present the light curves obtained during an 8 yr program of optical spectroscopic monitoring of nine Seyfert 1 galaxies: 3C 120, Akn 120, Mrk 79, Mrk 110, Mrk 335, Mrk 509, Mrk 590, Mrk 704, and Mrk 817. All objects show significant variability in both the continuum and emission-line fluxes. We use cross-correlation analysis to derive the sizes of the broad $H\beta$-emitting regions based on emission-line time delays, or lags. We successfully measure time delays for eight of the nine sources and find values ranging from about 2 weeks to a little over 2 months. Combining the measured lags and widths of the variable parts of the emission lines allows us to make virial mass estimates for the active nucleus in each galaxy. The virial masses are in the range 10^7–10^8 $M_\odot$.

Subject headings: galaxies: active — galaxies: Seyfert

1. INTRODUCTION

It has been known since the late 1960s that both the continuum (see, e.g., Fitch, Pacholczyk, & Weymann 1967) and broad emission lines (see, e.g., Andrillat & Collin-Souffrin 1968) in active galactic nuclei (AGNs) vary in flux with time. In the 1980s, spectroscopic monitoring programs showed that the continuum and emission-line variations are closely coupled, confirming that the emission-line regions are powered predominantly by photoionization by the central source. However, the typical emission-line response times were found to be surprisingly short compared to the light-travel times expected by most photoionization equilibrium models (see, e.g., Peterson et al. 1985b). Attempts were made to determine light-travel times for the broad-line region (BLR) by cross-correlation of continuum and emission-line fluxes (see, e.g., Gaskell & Sparke 1986), but the analyses were plagued by sparsely sampled light curves and relatively large uncertainties in the measured fluxes (see, e.g., Gaskell & Peterson 1987; Edelson & Krolik 1988). In spite of the difficulties, the potential for extracting physical information about the central regions of AGNs from variability was generally regarded to be enormous (see Peterson 1988 for a review of the early monitoring programs and their implications): in principle, it is possible to constrain significantly the structure and kinematics of the BLR by determining the emission-line response to continuum variations as a function of wavelength, since the broad lines are well resolved in radial velocity even at low (~ 10 Å) resolution. This process is known as "reverberation mapping" (Blandford & McKee 1982).

Late in the 1980s, it became possible to obtain the quality and quantity of data necessary to determine emission-line response times. In the ultraviolet, large amounts of *International Ultraviolet Explorer* time were devoted to AGN variability projects (see, e.g., Clavel et al. 1991). In the optical, CCDs became widely available on even moderate-size (~ 2 m) and small (~ 1 m) ground-based telescopes, making it possible to obtain high signal-to-noise ratio (S/N) spectra of high photometric accuracy with relative ease. The problem of poor time sampling was obviated by cooperation between observers, either by using many telescopes (see, e.g., Peterson et al. 1991) or by a group using a single facility (see, e.g., Maoz et al. 1990; Robinson 1994). Progress in reverberation mapping through 1992 is reviewed by Peterson (1993), and a more recent review is given by Netzer & Peterson (1997).

In 1988, we began a long series of approximately weekly spectroscopic monitoring of nearby bright Seyfert galaxies with a CCD spectrograph on the 1.8 m Perkins Telescope at Lowell Observatory. We present here the first analysis of most of these data. The scientific goals of the program have been:

1. To acquire optical continuum and emission-line light curves of sufficient sampling and quality to determine accurately the emission-line response times, or "lags," for a number of AGNs.

2. To investigate AGN continuum behavior over a long temporal baseline.

3. To investigate the nature of broad emission-line *profile* variability, and see what this reveals about the kinematics of the broad-line region.

4. To investigate the possibility of structural changes in the BLR on timescales of years (which corresponds to the dynamical time for the BLR).

Some of the results of this program have been reported elsewhere in the literature, but this is the first comprehensive presentation of the data obtained since 1988.

In this paper, we present the light curves for the optical continuum and the broad $H\beta$ emission lines in nine Seyfert galaxies. For most of these objects, we are able to determine accurately the emission-line lags, and for these objects we can estimate the mass of the central black hole. In future papers, we will discuss other issues, such as line-profile variations.

In § 2 we describe the observations and data reduction that led to this homogeneous database of spectra. Analysis of the light curves is described in § 3, and we summarize our results in § 4.

---

[1] Present address: School of Physics and Astronomy, University of St. Andrews, North Haugh, St. Andrews, Fife, KY16 9SS, Scotland; iw2@st-and.ac.uk.

[2] Postal address: Lowell Observatory, 1400 West Mars Hill Road, Flagstaff, AZ 86001; rayb@lowell.edu, rmw@lowell.edu.

TABLE 1

LIST OF SOURCES

SOURCE (1)	POSITION (1950.0)		z (4)	A_B (mag) (5)	L_λ (5100 Å) (ergs s^{-1} Å^{-1}) (6)
	α (2)	δ (3)			
Mrk 335......	00 03 45.2	+19 55 29	0.026	0.10	6.6×10^{39}
Mrk 590......	02 12 00.4	−00 59 58	0.026	0.05	5.4×10^{39}
3C 120........	04 30 31.6	+05 15 00	0.033	0.57	7.6×10^{39}
Akn 120	05 13 37.9	−00 12 15	0.033	0.40	1.5×10^{40}
Mrk 79	07 38 47.3	+49 55 41	0.022	0.23	4.5×10^{39}
Mrk 704......	09 15 39.4	+16 30 59	0.030	0.05	4.9×10^{39}
Mrk 110......	09 21 44.4	+52 30 08	0.035	0	4.0×10^{39}
Mrk 817......	14 34 57.9	+59 00 39	0.031	0	5.6×10^{39}
Mrk 509......	20 41 26.3	−10 54 18	0.034	0.18	1.6×10^{40}

NOTE.—Units of right ascension are hours, minutes, and seconds, and units of declination are degrees, arcminutes, and arcseconds.

2. OBSERVATIONS AND DATA REDUCTION

2.1. Sample Selection

The galaxies observed in this monitoring program were nonrigorously selected according to a number of simple criteria. These are among the brightest Seyfert 1 galaxies observable from the northern hemisphere. They are distributed fairly evenly in right ascension since the monitoring program was scheduled approximately one night per week throughout the entire year, and sources were observed whenever they were accessible. Many of these galaxies were found to have variable emission lines based on earlier observations (see, e.g., Peterson, Crenshaw, & Meyers 1985a, and references therein) with the Ohio State Image Dissector Scanner (OSU IDS; Byard et al. 1981). Some preference was given to galaxies in which the Hβ equivalent width had been observed to change, which was taken to be a possible indication that light travel-time effects might be important in these sources. Some consideration was also given to ensuring that a wide variety of broad-line profile types was represented in the sample.

In this paper, we report on results for the nine Seyfert galaxies listed in Table 1. The common source name is given in column (1), and the epoch 1950 right ascension and declination appear in columns (2) and (3), respectively. The redshift z is given in column (4), and the Galactic B-band extinction A_B, from the NED database,[3] is shown in column (5). Column (6) gives the specific luminosity at about 5100 Å in the rest frame of each galaxy, corrected for Galactic extinction, based on the average fluxes given later in this paper (Table 5).

In addition to the sources listed in Table 1, a number of other Seyfert galaxies were monitored spectroscopically as part of this program, often in coordination with other observers (particularly the International AGN Watch; Alloin et al. 1994) and often at multiple wavelengths. The well-studied source NGC 5548 has been one of our primary targets (Peterson et al. 1991, 1992, 1994; Korista et al. 1995), and recent observations are being prepared for publication. This program has also included observations of NGC 3783 (Stirpe et al. 1994), NGC 4151 (Kaspi et al. 1996a), NGC 7469 (Collier et al. 1998), and the broad-line radio galaxy 3C 390.3 (Dietrich et al. 1998), as well as Mrk 279 and NGC

4051 (to be published elsewhere). We have published preliminary results on two sources included here, Mrk 590 (Peterson et al. 1993) and Mrk 335 (Kassebaum et al. 1997); the results presented here include revisions of the data in these earlier papers, superseding the previous results. Our observations of another of these sources, Mrk 509, were included in a larger compilation (Carone et al. 1996), and here we present recent observations obtained since that program was completed. Our analysis incorporates data from Carone et al. (1996) as well.

Our sample does not include certain well-known nearby very low-luminosity AGNs; even at the time this program was initiated (1988), existing data suggested that weekly observations would seriously undersample the variations in these objects. Some of these lower luminosity objects were monitored by the LAG consortium (see Robinson 1994 for a compilation). Except for an intensive 10 day program in 1993 (Kaspi et al. 1996a), the best-known Seyfert 1, NGC 4151, has not been included as a priority target for this very reason.

We have also deliberately avoided higher luminosity sources for two reasons:

1. At the time this program was started, almost nothing was known about continuum and emission-line variability in high-luminosity nonblazar AGNs. The scientific focus of this program has been the use of emission-line variability to probe the inner structure of AGNs rather than the study of variability *per se*. We therefore decided to restrict our program to sources that we felt had the best chance of yielding useful variability data.

2. Higher luminosity sources tend to be at large redshifts. Inclusion of high-redshift sources in our program results in observations inefficiencies as the spectrograph grating angle has to be reset and the instrument recalibrated for higher redshift sources. This was deemed to be undesirable. We did briefly explore the possibility of including somewhat higher luminosity sources, and in early 1991, we observed GQ Comae approximately once per week for about 3 months. No continuum or emission-line variations were detected at that time. Since then, however, it has been demonstrated that higher luminosity AGNs do indeed undergo continuum and emission-line variations similar to those seen in the Seyfert galaxies discussed here (see, e.g., Kaspi et al. 1996b).

The reader is thus cautioned that the sources in Table 1 do not represent a statistical sample on any basis. They

---

[3] The NASA/IPAC Extragalactic Database (NED) is operated by the Jet Propulsion Laboratory, California Institute of Technology, under contract with the National Aeronautics and Space Administration.

were all selected for this program because we believed that the continuum and emission-line variability timescales were appropriate for 1 week sampling and because they were readily accessible in terms of position, redshift, and brightness. The sources in Table 1 span a mere factor of 4 in luminosity, while the AGN phenomenon extends over some 15 mag.

2.2. *Observations and Data Reduction*

All the observations were made with the Ohio State University CCD spectrograph on the 1.8 m Perkins Telescope of the Ohio Wesleyan and Ohio State universities at Lowell Observatory, near Flagstaff, Arizona. Observations were scheduled approximately once per week, year round, interrupted only by bad weather and occasional equipment failures. Each galaxy was observed whenever it was accessible, although special priority was assigned to NGC 5548 (discussed elsewhere), Mrk 335, Mrk 590, Akn 120, Mrk 79, and Mrk 509. Three of the sources discussed here, Mrk 110, Mrk 704, and Mrk 817, were added to the program relatively late, and Mrk 704 and 3C 120 were lower priority sources, so there are relatively fewer observations of these galaxies.

The entrance slit of the spectrograph was set to a fixed projected width of 5″0, and a projected extraction width of 7″6 was used. The large aperture was used to minimize seeing-dependent aperture effects (Peterson et al. 1995). The position angle of the slit was kept fixed at 90°. A grating ruled at 350 lines mm^{-1} was used, giving a dispersion of ~2 Å per pixel and a resolution of ~10 Å. During this program, two different CCDs were used: through 1991, a Texas Instruments model 4849 chip with 384 × 592 22 μm pixels, and from 1992 onward, a Tektronix 512 × 512 chip with 27 μm pixels. The wavelength range covered by the observations was somewhat larger than the 4600–5400 Å range used in this paper. Most observations were comprised of multiple (usually three) 20 minute integrations.

The bias subtraction, flat-field correction, wavelength calibration, and standard-star flux calibration were done in the standard way using the IRAF data reduction package. The wavelength calibration was based on either FeNe or HeAr discharge-tube spectra. Cosmic-ray hits were identified and removed to the fullest possible extent by comparison of individual exposures.

2.3. *Absolute Flux Calibration*

Absolute spectrophotometry of faint sources is a difficult task, as changes in atmospheric transparency and seeing highly influence the number of photons entering the spectrograph entrance aperture. Only rarely are conditions identical for observations of program objects and standard stars, and as a rule, spectrophotometric accuracy better than 10% is rarely achieved with ground-based observations. Seeing and transparency variations have weak wavelength dependence, however, so standard calibration techniques yield accurate *relative* spectrophotometry. In the case of Seyfert galaxies, *absolute* photometric accuracy can be achieved by using the narrow emission lines as internal flux standards, since these generally do not vary on the timescales of interest to us. The narrow emission lines arise in a spatially extended low-density region; long light-travel and recombination times (both typically 100–1000 yr) ensure that variations on much shorter timescales will not occur.

The absolute flux scale in each case is established by measuring the [O III] λ5007 flux in the minority of spectra that were obtained under photometric conditions, as judged by the observer on site and at the data reduction stage, where individual exposures were compared. In Table 2, we give the absolute fluxes that we have determined for the nine Seyfert galaxies in this study.

A potential problem with this method of flux calibration is that seeing-dependent aperture effects can be important, particular if the narrow-line region is spatially resolved and comparable in size to the projected entrance aperture of the instrument. It is in principle possible to correct for such effects by simulated aperture photometry of emission-line and host-galaxy images (Wanders et al. 1992; Peterson et al. 1995). However, none of the objects here has extended emission of sufficient strength to affect any of our results.

Once the absolute [O III] flux is determined for each source, we scale each spectrum by a multiplicative constant so that the [O III] flux in each spectrum of a given object is the same. We carry this out by comparing each spectrum to a high signal-to-noise ratio "reference" spectrum that is constructed by averaging all of the highest quality spectra and scaling this to the correct absolute flux. The scaling is accomplished by using the automatic scaling program developed by van Groningen & Wanders (1992), which performs the task in a fast, reliable, and objective way, and has been successfully used on a number of data sets. The program also corrects for small zero-point wavelength calibration errors between the individual spectra and takes resolution differences into account. The resulting set of calibrated spectra is therefore highly homogeneous. A few of the spectra were poorly focused, which made flux calibration very difficult and the results extremely suspect. These spectra were removed from the database.

All of the acceptable spectra were used to compute an average spectrum for each object. For each source, we also computed a root mean square (rms) spectrum, defined as

$$\sigma(\lambda) = \left\{ \frac{1}{(N-1)} \sum_{i=1}^{N} \left[F_i(\lambda) - \bar{F}(\lambda) \right]^2 \right\}^{1/2}, \qquad (1)$$

where the sum is taken over the N spectra, and $\bar{F}(\lambda)$ is the average spectrum. The rms spectrum is thus a measure of the variations around the mean, and constant features, such as narrow emission lines, Galactic absorption lines, and the nonvariable parts of the broad emission lines and the continuum, are eliminated. Any narrow-line residuals visible are due to imperfections in the data calibration. These are

TABLE 2
Absolute [O III] λ5007 Fluxes

Source (1)	Number of Observations (2)	Flux (10^{-13} ergs s^{-1} cm^{-2}) (3)
3C 120........	12	3.02 ± 0.16
Akn 120......	28	0.91 ± 0.04
Mrk 79.......	28	3.16 ± 0.19
Mrk 110......	26	2.26 ± 0.14
Mrk 335......	13	2.31 ± 0.10
Mrk 509......	13	6.79 ± 0.40[a]
Mrk 590......	17	1.04 ± 0.05
Mrk 704......	17	1.27 ± 0.07
Mrk 817......	20	1.34 ± 0.05

[a] From Carone et al. 1996.

usually very small (<1% in any given spectrum) but add up in the rms spectrum, often rendering them visible. The mean and rms spectra for these objects are shown in Figures 1, 2, and 3.

2.4. *Light Curve Measurements*

Once all of the spectra have been calibrated, continuum and emission-line flux measurements were made. For each object, the continuum flux is measured in a band about 15–20 Å wide at around 5100 Å in the rest frame of the object, as this is the most line-free region in this part of the spectrum. The exact wavelength limits used vary from object to object, depending on the strength and width of various emission lines, especially the Fe II blends.

The Hβ emission-line flux is measured in a simple fashion. First, an underlying continuum is interpolated between the local minima between He II λ4686 and Hβ on the short-wavelength side of Hβ and between Hβ and the Fe II blend on the long-wavelength side of Hβ. We then integrate the total flux above this continuum between the short-wavelength limit and a point just shortward of [O III] λ4959. This measurement includes some Fe II emission as well as the narrow-line Hβ component and misses Hβ flux
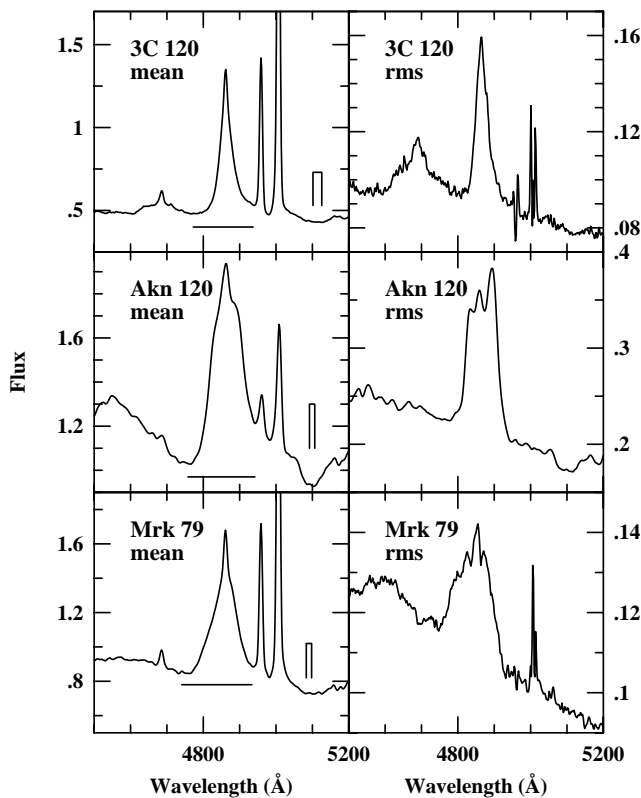

FIG. 1.—Average (*left column*) and rms (*right column*) spectra of 3C 120, Akn 120, and Mrk 79, based on the spectra reported here. The wavelength scale has been divided by (1 + z) to put each spectrum in the rest frame of the source. The strong broad line in the center is H$\beta\lambda$4861, and the narrow lines to the right are [O III] $\lambda\lambda$4959, 5007. In the left column, the horizontal line underneath Hβ shows the integration range for the line flux, and the bracketed region to the right shows the continuum region measured (as in Table 3). The broad He II λ4686 line is visible in some of the mean spectra, although it is often badly blended with Fe II lines. The rms spectra highlight the variable parts of the spectrum. In most cases, the He II λ4686 line is much more prominent in the rms spectrum than in the mean spectrum. The rms spectra also enhance the contrast of variable features in the line profiles, but also amplify residuals in the [O III] $\lambda\lambda$4959, 5007, which are used for flux calibration of these data.
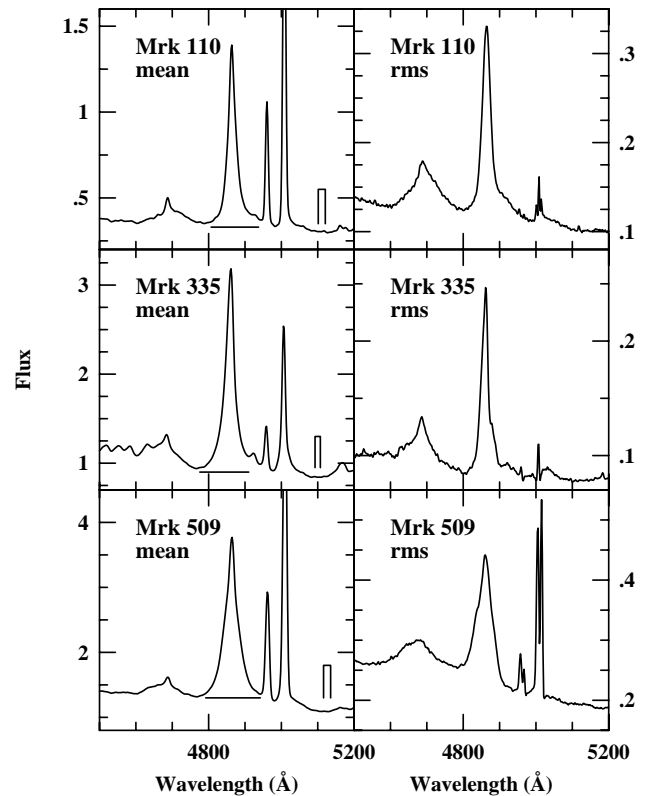

FIG. 2.—Average (*left column*) and rms (*right column*) spectra of Mrk 110, Mrk 335, and Mrk 509, based on the spectra reported here. The spectra are plotted as described in Fig. 1. The Mrk 509 mean and rms spectra are based on the 52 new spectra reported here, plus 95 spectra from the same instrument previously included in the presentation of Carone et al. (1996).

at high positive radial velocities, i.e., the extreme redward wing of the feature. However, this simple measurement is sufficiently good for our current goals and is model independent. The wavelength boundaries for the various integrations are given in Table 3. In each case, the wavelengths limits given are in the observed frame. Column (1) identifies the object, and column (2) gives the lower and upper bounds of the continuum region. The Hβ integration limits are given in column (3); the Hβ flux is taken to be the total flux above the linear pseudocontinuum defined by the limits given in column (4). In some, but not all, cases, He II emission can also be determined, and these measurements will

TABLE 3
INTEGRATION LIMITS

| OBJECT (1)	WAVELENGTH RANGE (Å)		
	Continuum (2)	Hβ (3)	Continuum Under Hβ (4)
3C 120.........	5270–5295	4930–5100	4925–5287
Akn 120	5260–5275	4915–5105	4905–5267
Mrk 79	5195–5210	4845–5042	4840–5202
Mrk 110......	5280–5300	4975–5110	4965–5290
Mrk 335......	5225–5240	4900–5038	4895–5232
Mrk 509......	5290–5310	4955–5110	4950–5300
Mrk 590......	5240–5260	4895–5045	4892–5250
Mrk 704......	5240–5255	4900–5080	4895–5252
Mrk 817......	5250–5275	4915–5090	4905–5262
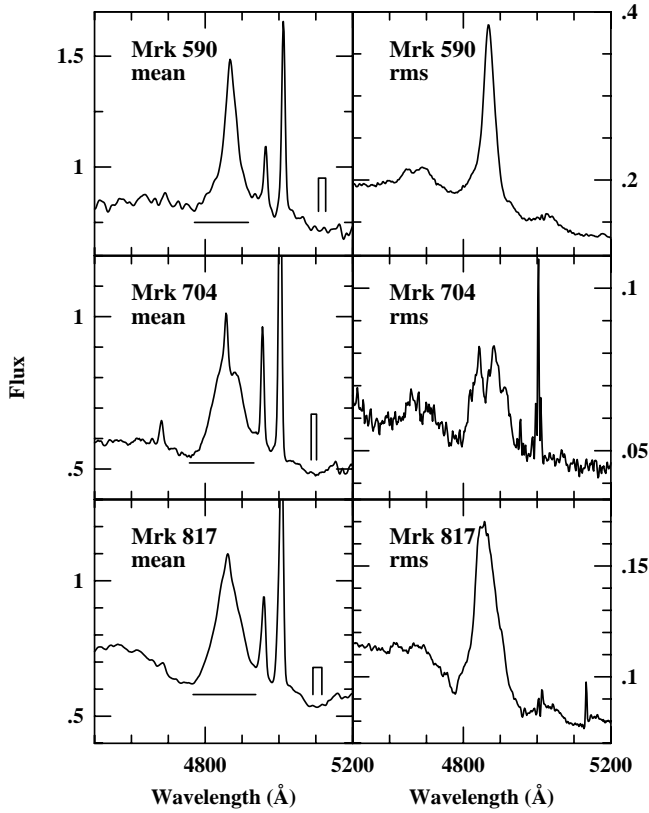
FIG. 3.—Average (*left column*) and rms (*right column*) spectra of Mrk 590, Mrk 704, and Mrk 817, based on the spectra reported here. The spectra are plotted as described in Fig. 1.

be reported elsewhere. It is also apparent from some of the rms spectra that some iron features, such as Fe II $\lambda5018$ in Mrk 335, Mrk 590, and Mrk 817, also have varied.

Assigning uncertainties to the light curve measurements is not straightforward, and we treat this problem in a heuristic manner. Most of the spectra have high signal-to-noise ratios (S/N $\gtrsim$ 50), and for these we assign uncertainties based on differences between observations that are closely spaced in time (within a few days of each other). This provides a conservative error estimate, since any real low-
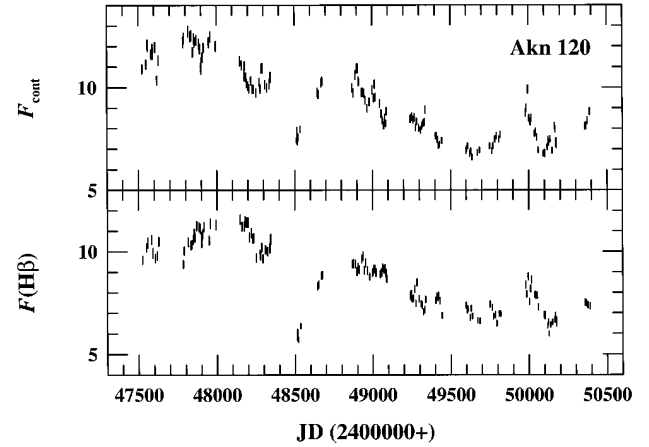

FIG. 5.—Light curves for Akn 120. *Upper panel*: Continuum, centered at 5099 Å in the rest frame of the source, in units of 10^{-15} ergs s^{-1} cm^{-2} Å^{-1}. *Lower panel*: Hβ emission line, in units of 10^{-13} ergs s^{-1} cm^{-2}.

amplitude amplitude variability is attributed to random error; the uncertainties may thus be somewhat smaller than those we assign by this method. We assign fractional errors of 0.02 to continuum and emission-line measurements.
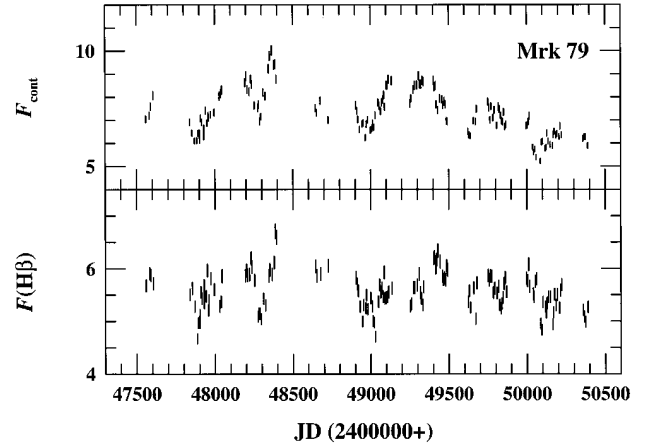

FIG. 6.—Light curves for Mrk 79. *Upper panel*: Continuum, centered at 5090 Å in the rest frame of the source, in units of 10^{-15} ergs s^{-1} cm^{-2} Å^{-1}. *Lower panel*: Hβ emission line, in units of 10^{-13} ergs s^{-1} cm^{-2}.
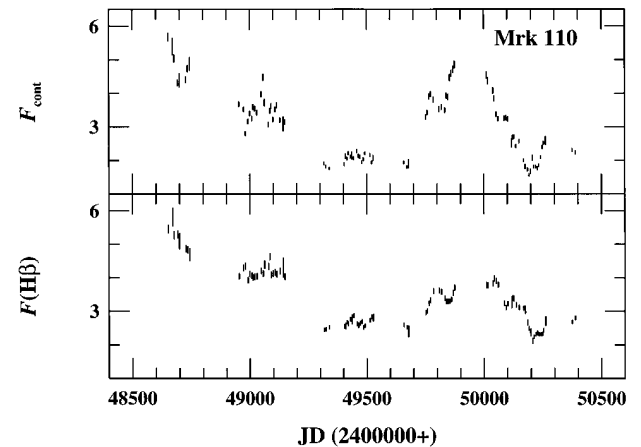

FIG. 4.—Light curves for 3C 120. *Upper panel*: Continuum, centered at 5114 Å in the rest frame of the source, in units of 10^{-15} ergs s^{-1} cm^{-2} Å^{-1}. *Lower panel*: Hβ emission line, in units of 10^{-13} ergs s^{-1} cm^{-2}.

FIG. 7.—Light curves for Mrk 110. *Upper panel*: Continuum, centered at 5111 Å in the rest frame of the source, in units of 10^{-15} ergs s^{-1} cm^{-2} Å^{-1}. *Lower panel*: Hβ emission line, in units of 10^{-13} ergs s^{-1} cm^{-2}.
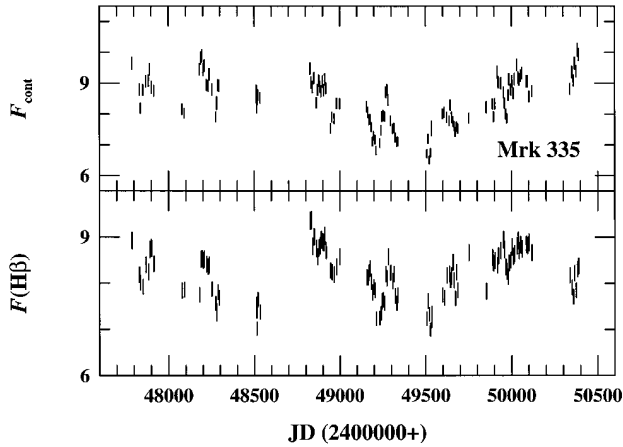
Fig. 8.—Light curves for Mrk 335. *Upper panel*: Continuum, centered at 5100 Å in the rest frame of the source, in units of 10^{-15} ergs s^{-1} cm^{-2} Å^{-1}. *Lower panel*: Hβ emission line, in units of 10^{-13} ergs s^{-1} cm^{-2}.

Fig. 11.—Light curves for Mrk 704. *Upper panel*: Continuum, centered at 5095 Å in the rest frame of the source, in units of 10^{-15} ergs s^{-1} cm^{-2} Å^{-1}. *Lower panel*: Hβ emission line, in units of 10^{-13} ergs s^{-1} cm^{-2}.

Some of the spectra, however, are of lower quality, usually because of abnormally short exposure times due to high airmass (at the beginning or end of an observing season for a particular source) or because of poor or highly
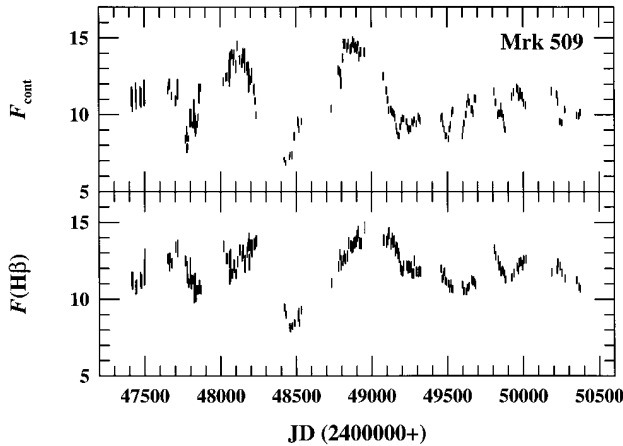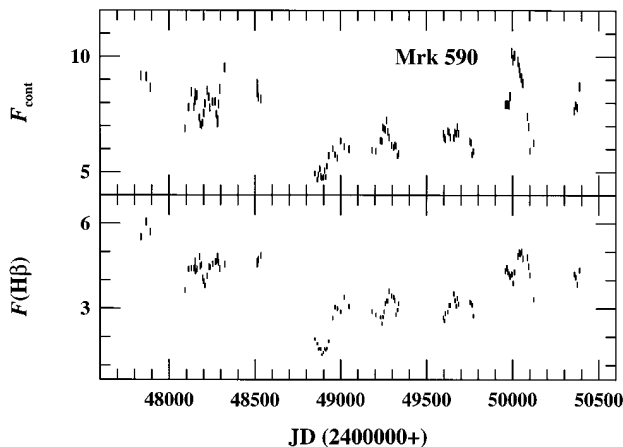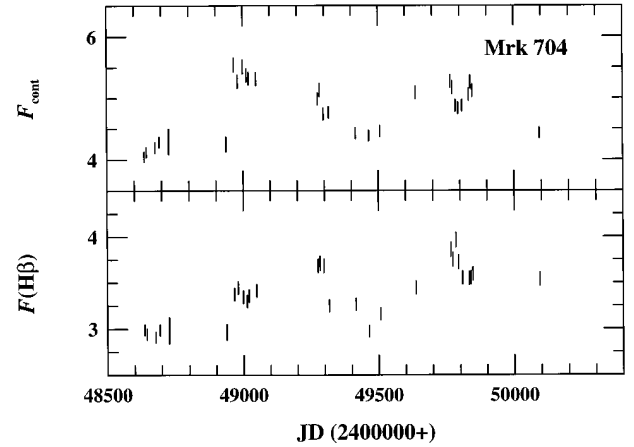

Fig. 9.—Light curves for Mrk 509. *Upper panel*: Continuum, centered at 5126 Å in the rest frame of the source, in units of 10^{-15} ergs s^{-1} cm^{-2} Å^{-1}. *Lower panel*: Hβ emission line, in units of 10^{-13} ergs s^{-1} cm^{-2}.

variable atmospheric transparency. To assign errors to these spectra, we first determine an apparent "signal-to-noise" ratio for each spectrum by computing the standard deviation of the flux values in the continuum band at about 5100 Å in the rest frame (this is usually based on 7–10 pixels). For high-quality data, this apparent S/N is lower than the actual signal-to-noise ratio of the spectra because weak emission and absorption structures are counted as random noise. For spectra with apparent S/N < 50, we assign a fractional error of 1/(S/N) to both the continuum and line measurements. We tested this procedure by first producing very high S/N spectra by averaging a large number of the highest quality spectra of each source and then performing Monte Carlo simulations in which we added random Gaussian-distributed noise to the spectrum and measured the continuum and emission-line fluxes in the same fashion as the real spectra. A large number of realizations for a given S/N revealed that the standard deviation of the measured fluxes was approximately equal to the mean flux divided by S/N. Thus, all continuum and emission-line flux measurements are taken to be accurate to ~2%, except those based on lower quality data, in which case the fractional errors in both the continuum and line fluxes are taken to be 1/(S/N).

Fig. 10.—Light curves for Mrk 590. *Upper panel*: Continuum, centered at 5117 Å in the rest frame of the source, in units of 10^{-15} ergs s^{-1} cm^{-2} Å^{-1}. *Lower panel*: Hβ emission line, in units of 10^{-13} ergs s^{-1} cm^{-2}.
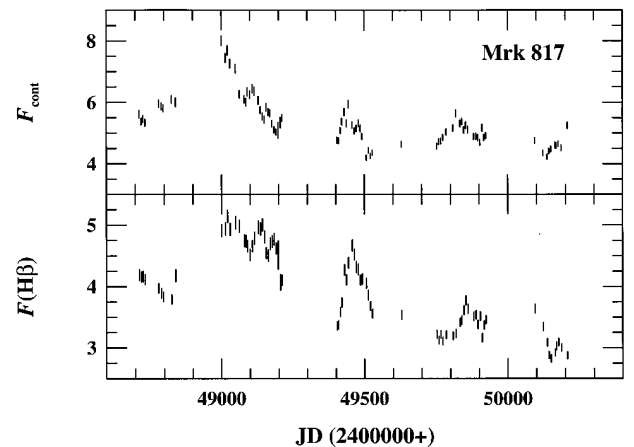

Fig. 12.—Light curves for Mrk 817. *Upper panel*: Continuum, centered at 5046 Å in the rest frame of the source, in units of 10^{-15} ergs s^{-1} cm^{-2} Å^{-1}. *Lower panel*: Hβ emission line, in units of 10^{-13} ergs s^{-1} cm^{-2}.

TABLE 4

SAMPLING STATISTICS

Source (1)	Number of Observations (2)	Span (days) (3)	$\langle \Delta T \rangle$ (days) (4)	ΔT_{med} (days) (5)
3C 120........	52	2206	50	11
Akn 120	141	2864	20	8
Mrk 79	143	2829	20	8
Mrk 110......	95	1737	18	8
Mrk 335......	123	2600	21	7
Mrk 509......	52	728	18	7[a]
Mrk 509......	194	2959	15	7[b]
Mrk 590......	102	2551	25	8
Mrk 704......	29	1457	52	20
Mrk 817......	81	1493	19	7

[a] New data only.
[b] New data and data from Carone et al. 1996.

The final light curves for the various objects are shown in Figures 4–12. The data can be obtained in tabular form through the World Wide Web.[4] All measurements are in the observer's frame and are uncorrected for Galactic extinction.

3. ANALYSIS AND DISCUSSION

3.1. Characteristics of the Database

The general sampling characteristics of the light curves plotted in Figures 4–12 are given in Table 4. Column (1) gives the source name and column (2) gives the total number of observations that comprise the light curve. Column (3) gives the number of days spanned by the observation, and the average and median intervals between observations are given in columns (4) and (5), respectively.

The primary targets (Akn 120, Mrk 79, Mrk 335, Mrk 509, and Mrk 590) are all well sampled, with median intervals between observations of 7–8 days for a span of 7–8 yr. The larger average intervals between observations are an effect of seasonal gaps that occur when the sources are near conjunction and thus unobservable. Of the other sources,

---

[4] The light curves and complete logs of observation are available in tabular form, in either PostScript or plain ASCII format, at http://www.astronomy.ohio-state.edu/~peterson/AGN/.

Mrk 110 and Mrk 817 are also well sampled, but for only 4–5 yr. Both 3C 120 and Mrk 704 are quite poorly sampled, as will become apparent when we carry out the time-series analysis.

All of the sources observed underwent significant continuum and emission-line variations. Statistics that describe the variations are given in Table 5. For each object, we give, for both the continuum and Hβ, the average flux $\langle F \rangle$ (cols. [2] and [5]), the normalized variability amplitude F_{var}, i.e., the rms fractional variability corrected for measurement uncertainties, as defined by Rodríguez-Pascual et al. (1997) (cols. [3] and [6]), and the ratio of maximum to minimum flux R_{max} (cols. [4] and [7]). The average continuum flux reported here is the value used to compute the luminosity given in Table 1. The variability parameters have not been corrected for the constant contaminants, starlight in the case of the continuum, and the Hβ narrow-line components in the case of the line. These issues are beyond the scope of this contribution and will be dealt with in the future.

3.2. Time-Series Analysis

The primary goal of this program has been to determine for each of these sources the time delay, or lag, between the continuum and Hβ flux variations. The existence of time delays is in most cases apparent from close inspection of the light curves. We quantify these time delays by cross-correlating the continuum and emission-line light curves for each object. Most of the light curves are well sampled, so the cross-correlation method that we use is the interpolation cross-correlation function (ICCF) introduced by Gaskell & Sparke (1986) and Gaskell & Peterson (1987). In cases where there are significant gaps in the data that may compromise the validity of linear interpolation between adjacent measurements, we have also employed the discrete-correlation function (DCF) method (Edelson & Krolik 1988) as a check on the results. The specific implementations of the ICCF and DCF that we employ are described by White & Peterson (1994).

The uncertainties in the cross-correlation results are estimated by using the model-independent FR/RSS Monte Carlo method described by Peterson et al. (1998). Each Monte Carlo simulation consists two parts, which are referred to as "random subset selection" (RSS) and "flux randomization" (FR). The RSS procedure consists of ran-

TABLE 5

VARIABILITY STATISTICS

SOURCE (1)	CONTINUUM			Hβ		
	$\langle F \rangle$[a] (2)	F_{var} (3)	R_{max} (4)	$\langle F \rangle$[b] (5)	F_{var} (6)	R_{max} (7)
3C 120.........	14.30 ± 0.77	0.178	2.34 ± 0.07	13.78 ± 0.37	0.095	1.65 ± 0.05
Akn 120.......	19.31 ± 1.74	0.186	1.93 ± 0.06	18.74 ± 1.62	0.184	2.03 ± 0.06
Mrk 79	17.31 ± 0.96	0.130	1.92 ± 0.05	15.56 ± 0.37	0.062	1.44 ± 0.04
Mrk 110.......	13.05 ± 1.02	0.334	3.64 ± 0.11	13.40 ± 0.85	0.249	2.74 ± 0.16
Mrk 335.......	18.44 ± 0.78	0.090	1.55 ± 0.04	18.21 ± 0.52	0.060	1.34 ± 0.04
Mrk 509[c]	19.65 ± 0.85	0.085	1.39 ± 0.04	10.89 ± 0.65	0.056	1.26 ± 0.04
Mrk 509[d]	10.92 ± 1.87	0.168	2.15 ± 0.06	11.94 ± 1.29	0.105	1.81 ± 0.06
Mrk 590.......	17.18 ± 1.35	0.187	2.18 ± 0.06	13.66 ± 1.05	0.286	4.37 ± 0.12
Mrk 704.......	14.84 ± 0.46	0.092	1.37 ± 0.04	13.39 ± 0.30	0.087	1.36 ± 0.04
Mrk 817.......	15.36 ± 0.78	0.144	1.91 ± 0.05	13.96 ± 0.66	0.166	1.82 ± 0.05

[a] In units of 10^{-15} ergs s^{-1} cm^{-2} Å^{-1}.
[b] In units of 10^{-13} ergs s^{-1} cm^{-2}.
[c] New data only.
[d] New data and data from Carone et al. 1996.

domly drawing from a light curve of N points a new sample of N points, chosen without regard to whether any particular point has been previously drawn. In this regard, RSS is reminiscent of a standard statistical "bootstrap," although it differs in that the temporal order of the points must be preserved. It is only *after* N points have been selected that the redundant selections are removed from the sample. This effectively reduces the number of points in each light curve by a factor of $\sim 1/e$. The RSS procedure thus accounts for the effects that individual data points may have on the cross-correlation by removing them at random. The second part of the procedure (FR) is intended to account for the effects of flux-measurement uncertainties. The observed fluxes are altered by random Gaussian deviates scaled to the uncertainty ascribed to each point. Peterson et al. (1998) demonstrate that, under a wide variety of fairly realistic conditions, the combined FR/RSS procedure yields conservative errors, in the sense that the real uncertainties may in fact be somewhat smaller than the errors quoted.

Cross-correlation calculations have been carried out using the entire data set for each source, and in most cases, also using data from single seasons (usually spanning about 200 days) in which the variability characteristics were favorable for accurate detection of a lag. The only data set that failed to yield a statistically significant lag estimate was that for Mrk 704, which is not surprising as this is the most poorly observed galaxy in our sample. Cross-correlation functions (CCFs) computed from each data set in its entirety are shown in Figure 13, which shows in each case the ICCF (continuous line) and the DCF (individual error bars). In each case, the ICCF and DCF are in excellent agreement near the peak, which is the area of interest. The ICCF and DCF often show disagreement for lags of 100 days or more, since it is in this regime where the large seasonal gaps become important and the underlying assumptions of the ICCF begin to break down. The peaks and centroids of the CCFs are, however, generally in good agreement.

The results of our cross-correlation analysis are presented in Table 6. Column (1) gives the object name, and the subset of the light curve used in the calculation is given in column (2). The ICCF centroid $\tau_{\rm cent}$ is given in column (3). The peak of the cross-correlation function occurs at a lag $\tau_{\rm peak}$ (col. [4]) and has value $r_{\rm max}$ (col. [5]). The FWHM of the ICCF is given in column (6), and the total number of observations in the light curve appears in column (7). The centroid $\tau_{\rm cent}$ is computed using all points with correlation coefficients $r \geq 0.8 r_{\rm max}$. The uncertainties given for $\tau_{\rm cent}$ and $\tau_{\rm peak}$ were computed with the FR/RSS methodology; a large number (~ 1000) of Monte Carlo realizations were used to build up a cross-correlation peak distribution (CCPD; Maoz & Netzer 1989), which is then integrated to given the uncer-
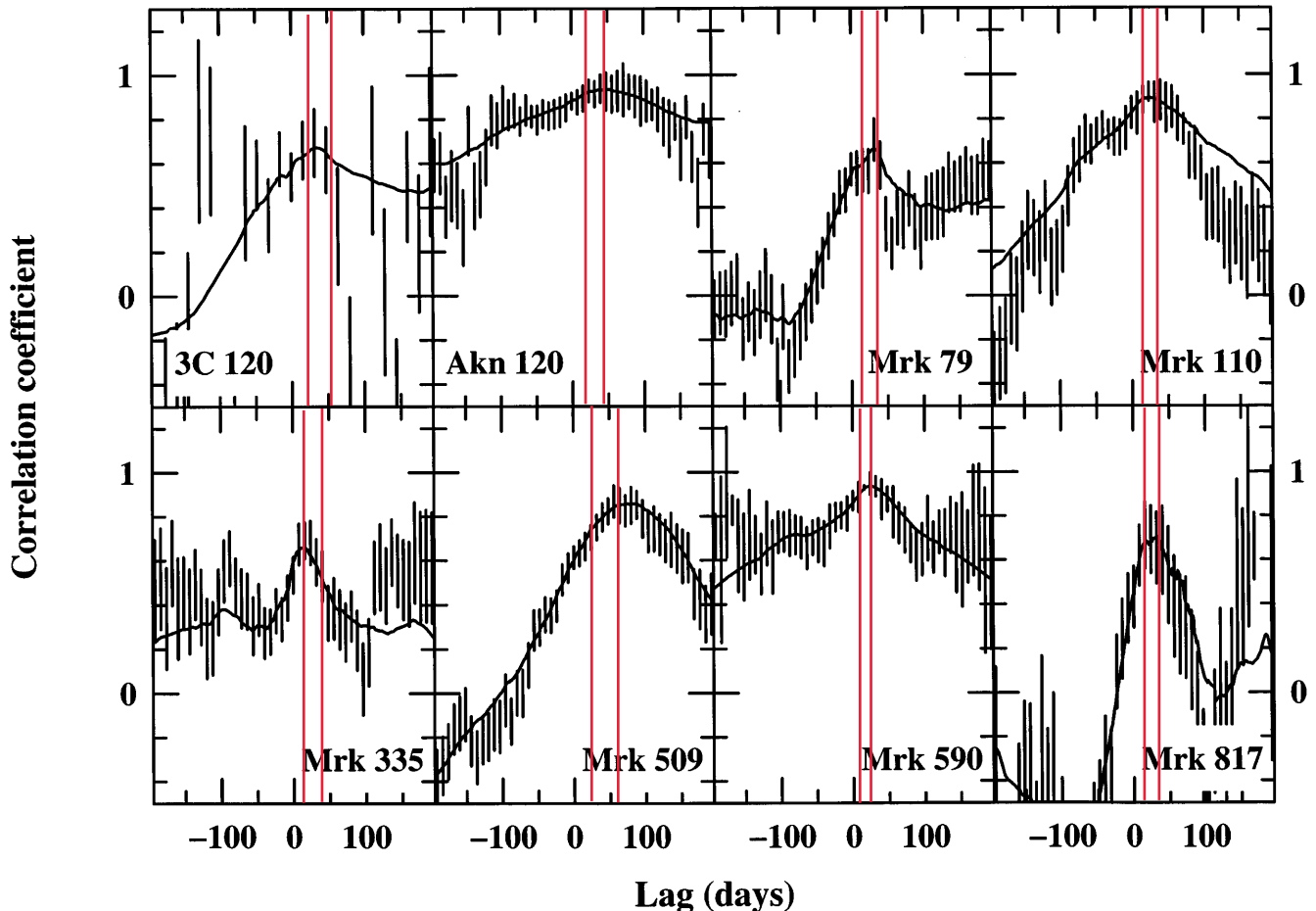

FIG. 13.—Cross-correlation functions based on the entire light curves shown in Figs. 4–10 and 12. The solid lines represent the interpolated cross-correlation function (ICCF) and the individual vertical lines show values of the discrete correlation function (DCF) and associated errors. The two methods are in good agreement on the timescales of interest, i.e., less than 100 days, which is where the CCFs peak in each case. Deviations at larger lags arise because of the gaps between observing seasons. Lags derived from the ICCFs are shown in Table 6. Of all the sources reported here, only the poorly sampled light curve of Mrk 704 failed to yield a statistically significant lag.

TABLE 6

CROSS-CORRELATION RESULTS

Source (1)	Subset (2)	τ_{cent} (days) (3)	τ_{peak} (days) (4)	r_{max} (5)	FWHM (days) (6)	Number of Obs. (7)
3C 120........	All data	$43.8^{+27.7}_{-20.3}$	34^{+10}_{-12}	0.674	406	52
Akn 120	All data	$60.2^{+31.1}_{-13.2}$	52^{+2}_{-14}	0.934	874	141
Akn 120	48149–48345	$49.5^{+12.4}_{-14.6}$	54^{+11}_{-16}	0.857	71	20
Akn 120	48870–49090	$31.6^{+14.1}_{-12.6}$	32^{+16}_{-14}	0.767	45	23
Akn 120	49981–50176	$38.6^{+5.3}_{-6.5}$	29^{+24}_{-1}	0.944	71	20
Mrk 79	All data	$25.7^{+11.7}_{-4.8}$	31^{+4}_{-6}	0.664	353	143
Mrk 79	47838–48044	$10.4^{+10.5}_{-11.4}$	14^{+9}_{-13}	0.622	44	20
Mrk 79	48193–48393	$18.1^{+4.9}_{-8.6}$	28^{+1}_{-21}	0.854	63	19
Mrk 79	48905–49135	$16.1^{+16.0}_{-7.0}$	15^{+19}_{-6}	0.702	61	23
Mrk 79	49996–50220	$41.6^{+6.2}_{-28.9}$	44^{+5}_{-33}	0.710	59	24
Mrk 110.....	All data	$31.6^{+9.0}_{-7.3}$	25^{+5}_{-5}	0.896	300	95
Mrk 110.....	48954–49149	$27.5^{+4.8}_{-23.9}$	27^{+6}_{-51}	0.746	24	21
Mrk 110.....	49752–49875	$19.5^{+6.5}_{-6.8}$	20^{+14}_{-6}	0.718	37	14
Mrk 110.....	50011–50262	$50.7^{+0.8}_{-27.5}$	24^{+6}_{-3}	0.969	213	28
Mrk 335.....	All data	$16.8^{+5.2}_{-3.3}$	12^{+7}_{-2}	0.660	112	123
Mrk 335.....	49156–49338	$15.6^{+6.9}_{-3.4}$	18^{+5}_{-9}	0.869	38	24
Mrk 335.....	49889–50118	$12.5^{+7.1}_{-5.1}$	15^{+5}_{-9}	0.791	30	25
Mrk 509......	All data[a]	$79.3^{+6.5}_{-6.2}$	86^{+1}_{-20}	0.858	216	194
Mrk 590......	All data	$22.5^{+17.8}_{-18.1}$	25^{+2}_{-2}	0.936	420	102
Mrk 590......	48090–48323	$20.5^{+4.5}_{-3.0}$	21^{+5}_{-4}	0.716	24	24
Mrk 590......	48848–49048	$15.7^{+9.0}_{-11.7}$	17^{+8}_{-11}	0.959	149	17
Mrk 590......	49183–49338	$28.7^{+7.2}_{-4.5}$	34^{+2}_{-12}	0.884	40	16
Mrk 590......	49958–50122	$28.5^{+5.0}_{-3.5}$	27^{+10}_{-2}	0.937	43	17
Mrk 817......	49404 onward	$27.0^{+10.1}_{-3.9}$	33^{+3}_{-15}	0.702	84	47
Mrk 817......	49000–49211	$19.5^{+4.5}_{-4.1}$	21^{+2}_{-6}	0.827	95	25
Mrk 817......	49404–49527	$15.5^{+4.3}_{-3.5}$	17^{+4}_{-5}	0.903	35	17
Mrk 817......	49752–49923	$36.3^{+8.0}_{-8.7}$	35^{+12}_{-7}	0.876	50	19

[a] New data and data from Carone et al. 1996.

tainties. The range of uncertainties contain 68% of the realizations, and thus would correspond to 1 σ uncertainties for a normal distribution.

Inspection of Table 6 shows that both τ_{peak} and τ_{cent} can vary considerably among the various subsets. While this might plausibly be ascribed to real physical changes in the structure of the BLR (see, e.g., Wanders 1995), the differences probably are simply indicative of a thick BLR (i.e., the ratio of outer to inner radius is much greater than unity). For a simple linear model of the line response $L(t)$, we can write

$$L(t) = \int \Psi(\tau)C(t - \tau)d\tau \,, \qquad (2)$$

which is known as the transfer equation, and $\Psi(\tau)$ is the transfer function (Blandford & McKee 1982), which depends on the BLR geometry, viewing angle (inclination to the line of sight), and the line-reprocessing physics. By convolving this with the continuum light curve $C(t)$, it is easy to show that the cross-correlation function (F_{CCF}) can be written

$$F_{CCF}(\tau) = \int \Psi(\tau')F_{ACF}(\tau - \tau')d\tau' \,, \qquad (3)$$

where F_{ACF} is the continuum autocorrelation function (Penston 1991; Peterson 1993). The CCF is thus sensitive to the particulars of the continuum variations. We performed some simple experiments by convolving the observed con-

tinuum light curves with model transfer functions for thick spherical shells. We found that it is relatively simple to obtain a wide range of lags if the geometry is thick and the response not strongly biased to particular radii. This point was first made by Netzer & Maoz (1990) to explain the large differences in the Hβ response determined by Peterson et al. (1991) and Netzer et al. (1990). Again, this is a topic that will be pursued more completely elsewhere.

In Table 7, we summarize the cross-correlation results. For τ_{cent}, we adopt the value that gives the smallest uncertainty for each source, and we adopt $c\tau_{cent}$ as an estimate of the BLR size. In the cases where subsets of the light curves yield the smallest FR/RSS error estimates, we show the

TABLE 7

BROAD-LINE REGION SIZE AND VIRIAL MASS ESTIMATES

Source (1)	τ_{cent} (days) (2)	v_{FWHM} (rms) (km s^{-1}) (3)	Mass ($10^7 M_\odot$) (4)
3C 120........	$43.8^{+27.7}_{-20.3}$	2300	13.4
Akn 120	$38.6^{+5.3}_{-6.5}$	5500	17.0
Mrk 79	$18.1^{+4.9}_{-8.6}$	6200	10.1
Mrk 110......	$19.5^{+6.5}_{-6.8}$	2500	11.8
Mrk 335......	$16.8^{+5.2}_{-3.3}$	1800	10.8
Mrk 509......	$79.3^{+6.5}_{-6.2}$	2800	19.0
Mrk 590......	$20.5^{+4.5}_{-3.0}$	2300	11.6
Mrk 817......	$15.5^{+4.3}_{-3.5}$	4100	13.8

cross-correlation functions based on the minimum-error subset in Figure 14. We have also measured the width of the broad Hβ line in the rms spectrum $v_{\rm FWHM}$, since this provides a measure of the radial velocity distribution of the gas that is actually varying. We adopt as a Keplerian velocity

$$v = \frac{\sqrt{3}}{2}\, v_{\rm FWHM} \qquad (4)$$

(Netzer 1990), and we use this to obtain a virial estimate of the mass of the central source:

$$M = \frac{v^2 c \tau_{\rm cent}}{G}\,. \qquad (5)$$

We give the virial mass for each source in column (4) of Table 7. These masses are highly uncertain since neither the geometry nor the kinematics of the BLR are known; indeed, we have assumed that the BLR velocity field is not primarily radial, which seems to be generally consistent with the reverberation results for other galaxies. In any case, equation (5) should contain a numerical factor of order unity that depends on the detailed geometry and kinematics of the BLR. Thus the masses given in Table 7 are valid only as order-of-magnitude estimates.

3.3. Comments on Individual Objects

We conclude this section with some brief comments on a few of the objects.

3.3.1. 3C 120

Continuum and emission-line variability was first reported in this source by Oke, Readhead, & Sargent (1980) and French & Miller (1980), who placed an upper limit on the size of the Hβ-emitting region of ~ 0.2 pc ≈ 240 light days. Our light curve is not particularly well sampled; however, we do find a statistically significant lag, but with a large formal uncertainty ($\tau_{\rm cent} = 43.8^{+27.7}_{-20.3}$ days).

3.3.2. Akn 120

The galaxy Akn 120 is of special interest to us, as it provided the original evidence that the BLR is more compact than was thought at the beginning of the last decade (Peterson et al. 1985b). Through the mid-1980s, we monitored Akn 120 regularly with the OSU IDS (see Peterson, Korista, & Wagner 1989, and references therein). Several problems prevented obtaining an accurate measurement of the lag:

1. The temporal sampling, originally selected on the assumption that the BLR was a light year or so in radius, was too poor to resolve the line response.
2. The typical uncertainties in the IDS measurements were $\sim 8\%$; short timescale, low-amplitude variations simply could not be detected.
3. The narrow [O III] $\lambda\lambda 4959$, 5007 lines are unusually weak in Akn 120 (see Figs. 1, 2, and 3), and flux calibration based on [O III] $\lambda 5007$ is less reliable than it is normally.
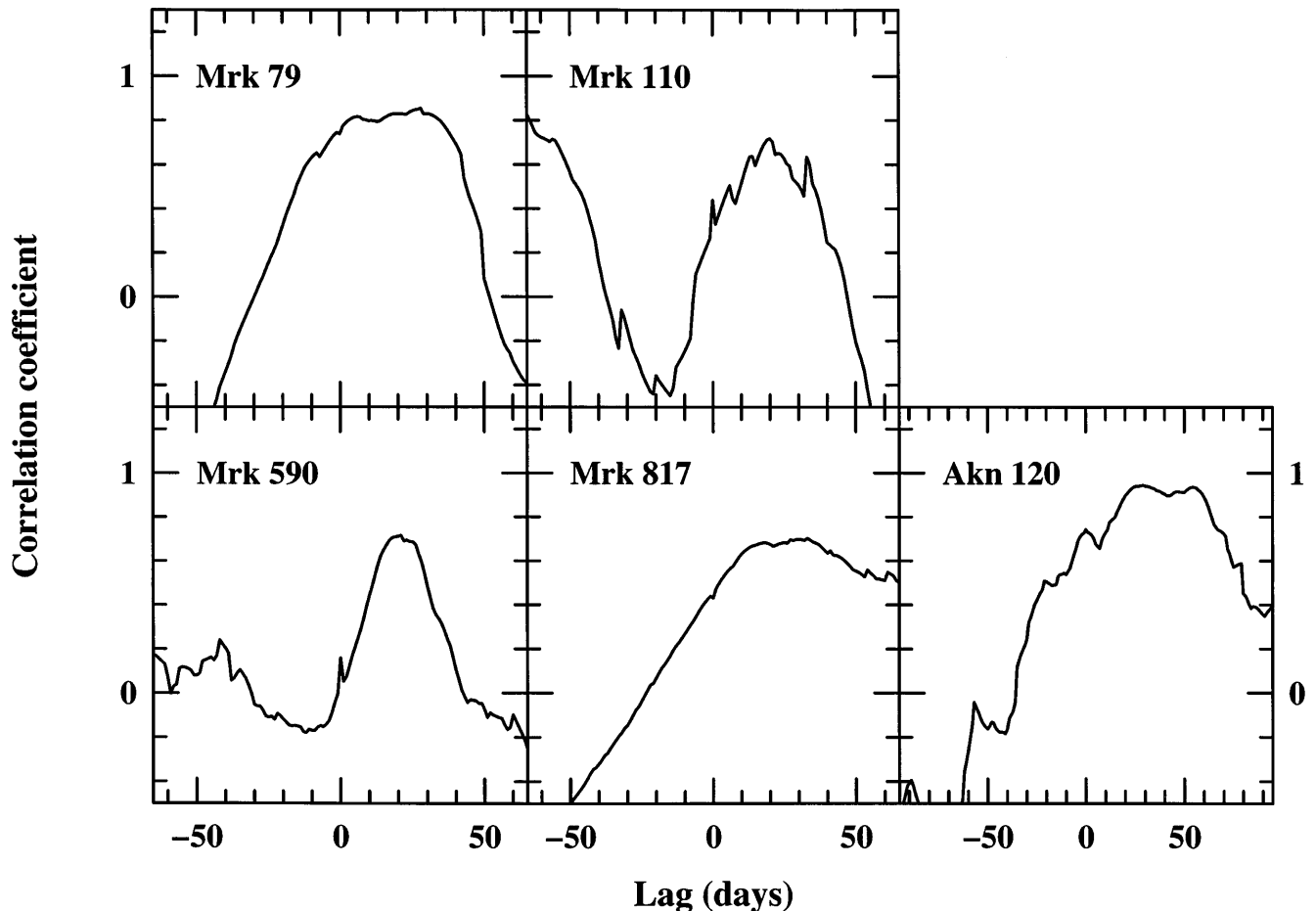

FIG. 14.—Cross-correlation functions based on the subsets that yield the smallest formal errors. Only the interpolation cross-correlation function is shown since these are based on too few points for the DCF to perform well (see White & Peterson 1994). Many of these CCFs show weak sharp features at $\tau = 0$, indicative of weakly correlated (positive peaks) or anticorrelated (negative peaks) errors.

This leads to systematic "correlated errors" in the continuum and emission-line fluxes at zero lag; i.e., any error in the [O III] $\lambda 5007$ calibration introduces a systematic error that drives the continuum and line fluxes in the same direction, thus artificially enhancing the cross-correlation at $t = 0$.

The large flux uncertainties presented the biggest problem with the earlier IDS data, since simulations suggested that the systematic correlated errors would not matter if the total error level could be decreased by a factor of 2 or more (Gaskell & Peterson 1987). In fact, replacement of the IDS spectrograph with the CCD spectrograph has decreased the uncertainties by a factor of 4.

The combined IDS and CCD continuum and Hβ light curves of Akn 120 are shown in Figure 15. The dramatic improvement in the signal-to-noise ratio of the light curves between the two instruments is readily apparent. It might seem disturbing that the amplitude of variability seems to have decreased with the advent of the improved instrument, but this type of behavior is seen in more homogeneous data as well. Mrk 509 (Fig. 9) shows a similar episode of violent variability followed by lower amplitude variations. Since it was these dramatic variations in Akn 120 that led us directly to programs such as reported here, we do not regard the difference between the variations seen in the early 1980s and those in the early 1990s as especially suspicious.

Figure 16 shows the result of cross-correlating the IDS continuum and Hβ light curves (also shown in Fig. 17 of Peterson et al. 1989). The centroid of the ICCF shown in Figure 16 is $\tau_{cent} = 8.7^{+9.9}_{-10.2}$ days, which is certainly erroneous because the systematic errors have not been included in the FR/RSS simulations. The sharp peak at zero lag demonstrates the strong influence of correlated errors in this source. Peterson, Korista, & Wagner point out that the asymmetric part of this function peaks at 51 ± 12 days, which is generally consistent with the results reported in Table 6, based on the higher quality CCD data. The asymmetric peak around zero lag is also found using the DCF method, also shown in Figure 16. This is contrary to what is stated by Edelson & Krolik (1988) because the version of
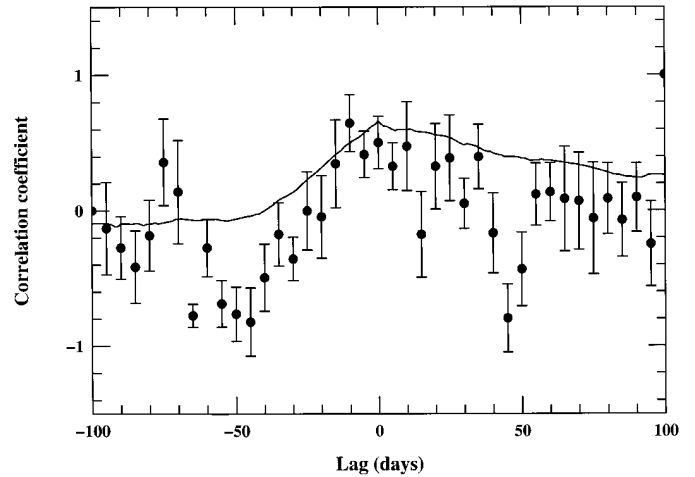
FIG. 16.—Cross-correlation functions for Akn 120, based on IDS data from Peterson et al. (1989) as shown in Fig. 14 (data points prior to JD 2447400). The solid line represents the interpolated cross-correlation function (ICCF), and the points with associated error bars are discrete correlation function (DCF) values. This should be compared with Fig. 5b of Edelson & Krolik (1988).

the DCF code used by Edelson & Krolik contained an error in how the data were weighted (see White & Peterson 1994, footnote 2). Our version of the DCF does not weight the data at all. Figure 16 should be compared directly with Figure 5b of Edelson & Krolik.

The cross-correlation lags that we obtain for Akn 120 are also generally consistent with the estimates of Gaskell & Peterson (1987; $\tau = 14 \pm 21$ days, based on a Monte Carlo model that included the effects of correlated errors) and of Peterson & Gaskell (1991; $\tau = 39 \pm 14$ days, based on combined UV/optical data obtained during the largest outburst).

3.3.3. Mrk 79

Markarian 79 has been included on our list of priority sources since the early 1980s, as our first observations with the OSU IDS showed it to be one of the highest amplitude variables in our survey (Peterson et al. 1985a). Like Akn 120 and NGC 5548, it was included in our monthly monitoring program in 1983–1985; these data failed to yield a cross-correlation lag, apparently because the light curves were badly undersampled (Peterson & Gaskell 1986). Oddly enough, over the 8 yr of our CCD-based program, Mrk 79 has been one of the *least* variable sources in our sample. The variations were sufficient, however, for a lag to be measured from the entire data set, as well as in four individual subsets.

3.3.4. Mrk 110

Our interest in Mrk 110 dates back to 1983–1984, when we observed an enormous change in the strength of He II $\lambda 4686$ in two spectra obtained a year apart (Peterson 1988). This behavior is also apparent in the rms spectrum of Mrk 110 shown in Figure 2.

3.3.5. Mrk 335

This galaxy was included in our sample on the basis of an earlier study by Shuder (1981) that suggested the variations would be well resolved by weekly monitoring. A preliminary analysis based on most of the data presented here was presented by Kassebaum et al. (1996). The light curves presented here supersede those presented by Kassebaum et al.,
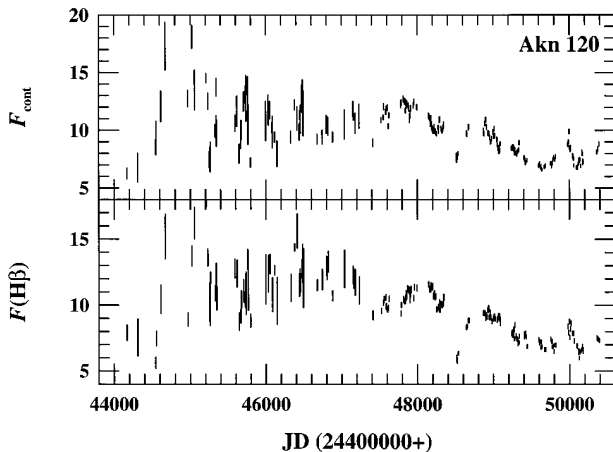

FIG. 15.—Combined light curves for Akn 120, including IDS data from Peterson et al. (1989), and CCD data, as in Fig. 5. The uncertainties in the CCD data are about 4 times smaller than the uncertainties in the IDS data. *Upper panel*: Continuum, centered at ~ 5100 Å in the rest frame of the source, in units of 10^{-15} ergs s^{-1} cm^{-2} Å^{-1}. *Lower panel*: Hβ emission line, in units of 10^{-13} ergs s^{-1} cm^{-2}.

but the cross-correlation results are not changed substantively by using the revised light curves.

3.3.6. Mrk 509

Most of the data presented here previously appeared in a large compilation by Carone et al. (1996). The new data presented here have simply been appended to the light curves presented by Carone et al. The mean and rms spectra shown in Figure 2, however, are based *only* on the OSU CCD spectra.

3.3.7. Mrk 590

Markarian 590 was included in our program because our early IDS observations showed that it underwent enormous Hβ variations. Additional observations indicated that the emission-line variations were concentrated in the core of the line; the wings apparently vary much less, leading Ferland, Korista, & Peterson (1990) to suggest that the high radial velocity Hβ emission arises in an optically thin gas. A preliminary version of a subset of our CCD observations (JD 2448090–2448323) has been previously published (Peterson et al. 1993).

3.3.8. Mrk 704 and Mrk 817

We included both of these sources as secondary targets rather late in the program, based on their positions in the sky and because they have interesting, complex Hβ profiles. Mrk 704 was too poorly sampled to yield a cross-correlation result; nevertheless, interesting profile variations were observed, as seen in the rms profiles in Figure 3. These will be discussed elsewhere.

4. CONCLUSIONS

In this contribution, we have reported on the initial results of an eight year spectroscopic monitoring program on Seyfert 1 galaxies. Most of these sources were observed nearly weekly whenever they were accessible, making these

and NGC 5548 (Peterson et al. 1994) especially well suited to the study of long-term continuum and emission variability in nonblazar AGNs. For the best-sampled galaxies in our sample, we have over 100 homogeneous spectra.

Of the nine sources presented in this paper, we were able to measure Hβ response times, or lags, for eight of them. The lags range from a little more than 2 weeks to more than 2 months, as summarized in Table 7. In many cases, the lags are measurable with data from individual observing seasons. These sometimes show variations from year to year, and this probably indicates that the BLR is physically thick, i.e., the outer radius of the BLR is much greater than the inner radius. We have combined the measured BLR response times with measured widths of the Hβ rms profiles to obtain virial mass estimates for the central source. These are all in the range 10^7–10^8 $M_\odot$.

REFERENCES

Alloin, D., Clavel, J., Peterson, B. M., Reichert, G. A., & Stirpe, G. M. 1994, in Frontiers of Space and Ground-Based Astronomy, ed. W. Wamsteker, M. S. Longair, & Y. Kondo (Dordrecht: Kluwer), 423
Andrillat, Y., & Collin-Souffrin, S. 1968, Astrophys. Lett., 1, 111
Blandford, R. D., & McKee, C. F. 1982, ApJ, 255, 419
Byard, P. L., Foltz, C. B., Jenkner, H., & Peterson, B. M. 1981, PASP, 93, 147
Carone, T. E., et al. 1996, ApJ, 471, 737
Clavel, J., et al. 1991, ApJ, 366, 64
Collier, S. J., et al. 1998, ApJ, in press
Dietrich, M., et al. 1998, ApJS, 115, 185
Edelson, R. A., & Krolik, J. H. 1988, ApJ, 333, 646
Ferland, G. J., Korista, K. T., & Peterson, B. M. 1990, ApJ, 363, L21
Fitch, W., Pacholczyk, A. G., & Weymann, R. J. 1967, ApJ, 150, L67
French, H. B., & Miller, J. S. 1980, PASP, 92, 753
Gaskell, C. M., & Peterson, B. M. 1987, ApJS, 65, 1
Gaskell, C. M., & Sparke, L. S. 1986, ApJ, 305, 175
Kaspi, S., Smith, P. S., Maoz, D., Netzer, H., & Jannuzi, B. T. 1996a, ApJ, 471, L75
Kaspi, S., et al. 1996b, ApJ, 470, 336
Kassebaum, T. M., Peterson, B. M., Wanders, I., Pogge, R. W., Bertram, R., & Wagner, R. M. 1997, ApJ, 475, 106
Korista, K. T., et al. 1995, ApJS, 97, 285
Maoz, D., & Netzer, H. 1989, MNRAS, 236, 21
Maoz, D., et al. 1990, ApJ, 351, 75
Netzer, H. 1990, in Active Galactic Nuclei, ed. R. D. Blandford, H. Netzer, & L. Woltjer (Berlin: Springer), 137
Netzer, H., & Maoz, D. 1990, ApJ, 365, L5
Netzer, H., & Peterson, B. M. 1997, in Astronomical Time Series, ed. D. Maoz, A. Sternberg, & E. Leibowitz (Dordrecht: Kluwer), 85
Netzer, H., et al. 1990, ApJ, 353, 108

Oke, J. B., Readhead, A. C. S., & Sargent, W. L. W. 1980, PASP, 92, 758
Penston, M. V. 1991, in Variability of Galactic Nuclei, ed. H. R. Miller & P. J. Wiita (Cambridge: Cambridge Univ. Press), 343
Peterson, B. M. 1988, PASP, 100, 18
———. 1993, PASP, 105, 247
Peterson, B. M., Ali, B., Horne, K., Bertram, R., Lame, N. J., Pogge, R. W., & Wagner, R. M. 1993, ApJ, 402, 469
Peterson, B. M., Crenshaw, D. M., & Meyers, K. A. 1985a, ApJ, 298, 283
Peterson, B. M., & Gaskell, C. M. 1986, AJ, 92, 552
———. 1991, ApJ, 368, 152
Peterson, B. M., Korista, K. T., & Wagner, R. M. 1989, AJ, 98, 500
Peterson, B. M., Meyers, K. A., Capriotti, E. R., Foltz, C. B., Wilkes, B. J., & Miller, H. R. 1985b, ApJ, 292, 164
Peterson, B. M., Pogge, R. W., Wanders, I., Smith, S. M., & Romanishin, W. 1995, PASP, 107, 579
Peterson, B. M., Wanders, I., Horne, K., Collier, S., Alexander, T., & Kaspi, S. 1998, PASP, in press
Peterson, B. M., et al. 1991, ApJ, 368, 119
———. 1992, ApJ, 392, 470
———. 1994, ApJ, 425, 622
Robinson, A. 1994, in Reverberation Mapping of the Broad-Line Region in Active Galactic Nuclei, ed. P. M. Gondhalekar, K. Horne, & B. M. Peterson (San Francisco: ASP), 147
Rodríguez-Pascual, P. M., et al. 1997, ApJS, 110, 9
Shuder, J. M. 1981, AJ, 86, 1595
Stirpe, G. M., et al. 1994, ApJ, 425, 609
van Groningen, E., & Wanders, I. 1992, PASP, 104, 700
Wanders, I. 1995, A&A, 296, 332
Wanders, I., Peterson, B. M., Pogge, R. W., DeRobertis, M. M., & van Groningen, E. 1992, A&A, 266, 72
White, R. J., & Peterson, B. M. 1994, PASP, 106, 879